

# AGU Advances

## RESEARCH ARTICLE

10.1029/2025AV001701

**Peer Review** The peer review history for this article is available as a PDF in the Supporting Information.

### Key Points:

- We resolve rupture processes of  $40 M > 7$  deep earthquakes and compare them with thermal and compositional structure in seven subduction zones
- Deep quakes likely nucleate via olivine transformation in the cold slab core and propagate beyond the core as shear thermal instability
- Dual mechanism transition leads to larger moment release, complex rupture geometry, and higher stress drops

### Supporting Information:

Supporting Information may be found in the online version of this article.

### Correspondence to:

Z. Jia,  
[zjia@ig.utexas.edu](mailto:zjia@ig.utexas.edu)

### Citation:

Jia, Z., Fan, W., Mao, W., Shearer, P. M., & May, D. A. (2025). Dual mechanism transition controls rupture development of large deep earthquakes. *AGU Advances*, 6, e2025AV001701. <https://doi.org/10.1029/2025AV001701>

Received 15 FEB 2025

Accepted 28 APR 2025

### Author Contributions:

**Conceptualization:** Zhe Jia, Wenyuan Fan, Peter M. Shearer

**Data curation:** Zhe Jia, Wenyuan Fan, Wei Mao

**Formal analysis:** Zhe Jia, Wenyuan Fan, Wei Mao, Peter M. Shearer

**Funding acquisition:** Zhe Jia, Wenyuan Fan, Peter M. Shearer, Dave A. May

**Investigation:** Zhe Jia, Wenyuan Fan, Wei Mao, Peter M. Shearer, Dave A. May

**Methodology:** Zhe Jia, Wenyuan Fan, Wei Mao, Peter M. Shearer, Dave A. May

© 2025. The Author(s).

This is an open access article under the terms of the [Creative Commons](#)

[Attribution License](#), which permits use, distribution and reproduction in any medium, provided the original work is properly cited.

## Dual Mechanism Transition Controls Rupture Development of Large Deep Earthquakes

Zhe Jia<sup>1,2</sup> , Wenyuan Fan<sup>2</sup> , Wei Mao<sup>3,4</sup>, Peter M. Shearer<sup>2</sup> , and Dave A. May<sup>2</sup> 

<sup>1</sup>Institute for Geophysics, Jackson School of Geosciences, UT Austin, Austin, TX, USA, <sup>2</sup>Scripps Institution of Oceanography, UC San Diego, La Jolla, CA, USA, <sup>3</sup>State Key Laboratory of Earth System Numerical Modeling and Application, College of Earth and Planetary Sciences, University of Chinese Academy of Sciences, Beijing, China, <sup>4</sup>Seismological Laboratory, California Institute of Technology, Pasadena, CA, USA

**Abstract** Deep earthquakes at depths below 500 km are under prohibitive pressure and temperature conditions for brittle failure. Individual events show diverse rupture behaviors and a coherent mechanism to explain their rupture nucleation, propagation, and characteristics has yet to be established. We systematically resolve the rupture processes of 40 large  $M > 7$  deep earthquakes from 1990 to 2023 and compare the rupture details to their local metastable olivine wedge (MOW) structures informed from thermo-mechanical simulations in seven subduction zones. Our results suggest that these events likely initiate from metastable olivine transformations within the cold slab core and rupture beyond the MOW due to sustained weakening from molten rock at the rupture tip. Over half of the  $M > 7$  earthquakes likely rupture beyond the MOW boundary and are controlled by both mechanisms. Rupturing outside the MOW boundary leads to greater moment release, increased geometric complexity, and a reduction in rupture length, causing greater stress drops.

**Plain Language Summary** Deep earthquakes at depths of 500–700 km pose a long-standing mystery, as the extreme pressure and temperature conditions at these depths should prevent the brittle failure mechanisms that generate shallow earthquakes. Despite decades of observations and various proposed theories, a coherent mechanism that accounts for a range of deep earthquake magnitudes across different subduction zones has yet to be identified. In this study, we systematically analyze 40 large deep earthquakes worldwide with magnitudes greater than 7 and compare their rupture characteristics with thermal simulations of 7 subducting slabs hosting these events. We find that most large deep quakes are governed by a dual-mechanism transition process: rupture initiates through a mineral phase change (metastable olivine transformation) within the cold slab core and then continues rupturing beyond the core, facilitated by shear thermal runaway, ultimately allowing earthquakes to grow larger and release more stress. This dual mechanism transition provides a unified explanation for deep earthquake characteristics across diverse subduction environments, from the coldest slabs such as Tonga, to the warmest, including those beneath South America.

## 1. Introduction

Deep earthquakes occurring at depths between 500 and 700 km challenge our understanding of earthquake physics. At these depths, the extreme confining pressure and high temperature are prohibitive for brittle failure and frictional sliding, which drive typical shallow earthquakes (Green & Houston, 1995; Zhan, 2020). However, earthquakes with magnitudes (M) greater than 7 occur at these depths almost every year (Ekström et al., 2012). These deep seismic events share similar source characteristics to crustal earthquakes, such as double-couple focal mechanisms and a Gutenberg-Richter magnitude-frequency distribution (Frohlich, 1989; Gutenberg & Richter, 1956). Deep earthquakes occur exclusively at subduction zones, and knowing their physical mechanisms can provide unique constraints on the geometry, structure, and dynamics of subducting slabs and the surrounding mantle structure near the 660-km discontinuity (Billen, 2008; Hayes et al., 2018; Isacks & Molnar, 1971; Myhill, 2013). Multiple competing mechanisms have been proposed to explain deep earthquake occurrence. However, a coherent mechanism that can explain the diversity of deep event properties has yet to be identified.

Observations of the rupture propagation and spatial extent of deep earthquakes provide constraints on their governing mechanisms. For example, the early stages of the 1994 Fiji  $M_W$  7.5 and the 2013 Okhotsk  $M_W$  8.3 deep earthquakes appear to rupture in similar ways to shallow earthquakes, with rupture lengths comparable to those of cold slab cores, yielding low stress drops during their initial ruptures (Tibi et al., 1999; Wiens et al., 1994; Ye et al., 2013; Zhan et al., 2014). These rupture characteristics can be explained by the transformational faulting

**Project administration:** Zhe Jia, Wenyuan Fan, Peter M. Shearer  
**Resources:** Zhe Jia, Wenyuan Fan, Peter M. Shearer, Dave A. May  
**Software:** Zhe Jia  
**Supervision:** Zhe Jia, Wenyuan Fan, Peter M. Shearer  
**Validation:** Zhe Jia, Wenyuan Fan, Peter M. Shearer, Dave A. May  
**Visualization:** Zhe Jia, Wenyuan Fan, Peter M. Shearer, Dave A. May  
**Writing – original draft:** Zhe Jia  
**Writing – review & editing:** Zhe Jia, Wenyuan Fan, Wei Mao, Peter M. Shearer, Dave A. May

mechanism, which involves a phase transition of metastable olivine to wadsleyite or ringwoodite in the transition zone (depths of approximately 410–660 km) within the highly stressed, cold slab cores. This phase transition can create a weak zone and trigger shear faulting, leading to earthquake nucleation and rupture propagation (Burnley et al., 1991; Green & Burnley, 1989; Kirby, 1987). Importantly, this phase transition is controlled by temperature (Quinteros & Sobolev, 2012; Schmeling et al., 1999), and its temperature dependence defines a metastable olivine wedge (MOW). A MOW has been directly imaged in the Japan subducting slab (Kawakatsu & Yoshioka, 2011; Shen & Zhan, 2020). Additionally, laboratory experiments on olivine at realistic pressure and temperature conditions have successfully reproduced transformational faulting and rupture nucleation (Schubnel et al., 2013; Wang et al., 2017). However, the transformational faulting mechanism alone cannot fully explain all deep earthquakes. For example, the likely extent of MOWs is insufficient to accommodate the large ruptures of the 1994 Fiji and the 2013 Okhotsk events, suggesting additional processes that facilitate large earthquake rupture propagation (McGuire et al., 1997; Meng et al., 2014).

The thermal runaway mechanism is another process that can drive deep earthquakes (Green & Houston, 1995; Zhan, 2020). This mechanism involves localized shear heating that weakens the rock, producing a molten shear band that lubricates the fault and sustains rupture propagation (Ogawa, 1987; Karato et al., 2001). The thermal runaway mechanism is distinct from transformational faulting in that the latter involves shear dislocation along phase-transition generated weak zones, while the former results from localized heating that alters the frictional behavior of the fault. The thermal runaway mechanism has been used to explain some large deep earthquakes, such as the 1994 Bolivia  $M_w$  8.2 earthquake. This event occurred in the warm South American slab, which had a limited supply of metastable olivine at the event depth, thus excluding the possibility of a pure transformational faulting mechanism driving the earthquake (Kirby et al., 1996; Mosenfelder et al., 2001). The Bolivia event likely ruptured a compact area and had a particularly high stress drop (Frohlich, 2006; Kikuchi & Kanamori, 1994; Silver et al., 1995; Zhan et al., 2014), leading to the dissipation of most of its strain energy near the source (Kanamori et al., 1998), which may have triggered a shear thermal instability. However, shear thermal runaway alone cannot explain all deep earthquakes. For example, the 2018 Tonga-Fiji  $M_w$  8.2 earthquake originated within the slab core and ruptured in two stages, each showing distinct characteristics in extent and high-frequency radiation (Fan et al., 2019; Jia, Shen, et al., 2020). These variations highlight the complexity of deep earthquakes.

Here, we conduct a comprehensive analysis of rupture processes for all large, deep earthquakes worldwide ( $M > 7.0$ ) from 1990 to 2023. We derive subevent models to constrain the rupture propagations and dimensions of 40 deep events. By performing the same analysis for these events, we can identify statistically significant rupture variations to infer their driving mechanisms. Additionally, we model the local MOW structure across 31 profiles at seven subduction zones to examine the influence of the phase transformation mechanism on the rupture characteristics of deep earthquakes. Our results indicate that larger deep earthquakes often rupture beyond the confines of the MOWs. We find that, with increasing magnitude, deep earthquakes have larger stress drops and increased complexity in fault geometry and slip orientation. Collectively, these observations suggest a transition in rupture mechanism as earthquake moment increases, shifting from transformational faulting to shear thermal runaway. This mechanism transition is primarily determined by the ratio of the MOW width to the rupture extent. Our proposed mechanism transition connects two seemingly contradictory hypotheses and provides a coherent explanation for the varying rupture characteristics of large deep earthquakes.

## 2. Rupture Processes of Global $M_w > 7$ Deep Earthquakes

We image the rupture processes and dimensions of 40  $M > 7.0$  large deep earthquakes that have occurred from 1990 to 2023 (Figure 1). We develop a new subevent inversion method and model each deep earthquake as a sequence of point-source subevents, resolving their locations, timing, and focal mechanisms. This flexible parameterization can effectively resolve complex ruptures across multiple faults with varying geometries. In comparison to nonlinear Bayesian methods (Jia, Shen, et al., 2020; Jia, Wang, & Zhan, 2020; Jia et al., 2022; Kikuchi & Kanamori, 1991; Shi et al., 2018), our new method is computationally efficient, permitting systematic analysis of many large deep earthquakes. We linearly invert teleseismic P and SH waves to obtain moment tensor solutions of subevents for each earthquake. The location and timing of these subevents are characterized by an assumed unilateral rupture propagation, where we resolve the rupture directivity and velocity using a grid-search approach. Physically, only a limited region will slip at any given time during an earthquake, and thus earthquake ruptures can be approximated as a few subevents (Kikuchi & Kanamori, 1991; Lay et al., 2012; Yue & Lay, 2020). We overparameterize the inverse problem and apply this physics-based sparsity constraint to resolve

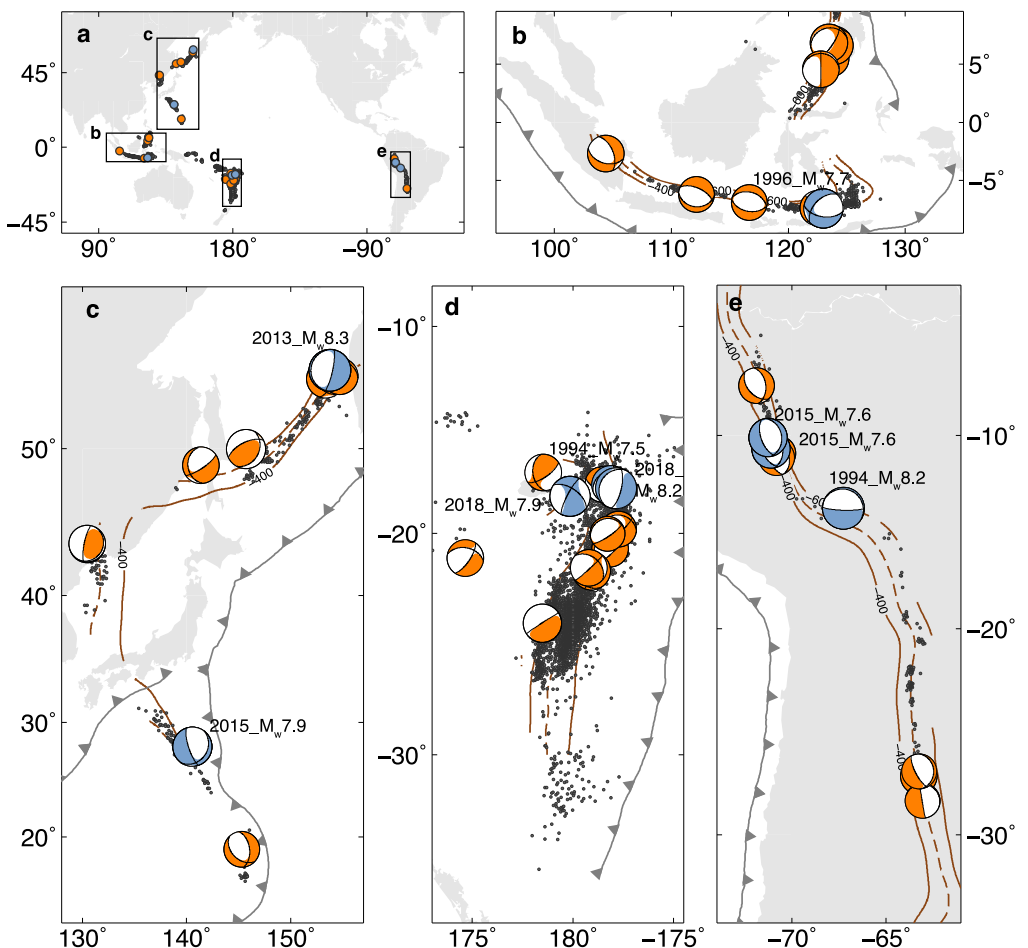


**Figure 1.** Global deep earthquakes with moment magnitude greater than 7.0 from 1990 to 2023. (a) Global distribution of analyzed large deep earthquakes, indicated by blue and orange circles. Subsequent panels detail the events in (b) Sumatra-Philippines, (c) Kuril-Honshu-Bonin, (d) Tonga, and (e) South America subduction zones. Focal mechanisms (beachballs) are from the Global Centroid Moment Tensor (GCMT) catalog. Events analyzed in previous case studies are colored in blue. Black dots indicate the historical deep (500–700 km) seismicity in the study regions. Slab depth contours are from the Slab 2 model (Hayes et al., 2018).

the earthquake subevents (Fan et al., 2014; Yao et al., 2011). Please see the Supporting Information S1 for more details (Nissen-Meyer et al., 2014; Van Driel et al., 2015).

We model the subevents at the hypocentral depth of the earthquake (Goes & Ritsema, 1995; Kikuchi & Kanamori, 1994; Zhan et al., 2014). Most target earthquakes occurred in remote regions without stations directly above the events. This lack of nearby stations causes trade-offs between resolving the subevent timing and depth when solely using downgoing teleseismic body waves. Depth phases such as pP and sS phases provide insights into vertical rupture propagation (Chen & Wen, 2015; Jia, Shen, et al., 2020). However, the complexities of ocean bottom reflections, water reverberations, and heterogeneous subduction zones can significantly distort depth phases, limiting their capability for unified comparison of large deep earthquake ruptures. Fixing the subevents at the hypocentral depth can stabilize the inversion and is a useful approximation for robustly estimating the horizontal rupture length of the earthquakes (Jia, Shen, et al., 2020; Zhan et al., 2014). Taking the 2018 Mw 8.2 Fiji earthquake as an example, we find that the fixed-depth inversion and the inversion with 20 km shallow-propagating ruptures yield similar horizontal rupture patterns and nearly identical waveform misfits (Figure S1 in Supporting Information S1), indicating that uncertainty in vertical rupture extent does not significantly impact our estimates of horizontal rupture dimensions. We further validate our results by comparing our models with nine published models obtained using different methods (Kikuchi & Kanamori, 1994; Wei et al., 2013; Ye, Lay, Zhan, et al., 2016; Zhan et al., 2014), some of which used depth phases to resolve source depths (Jia, Shen,

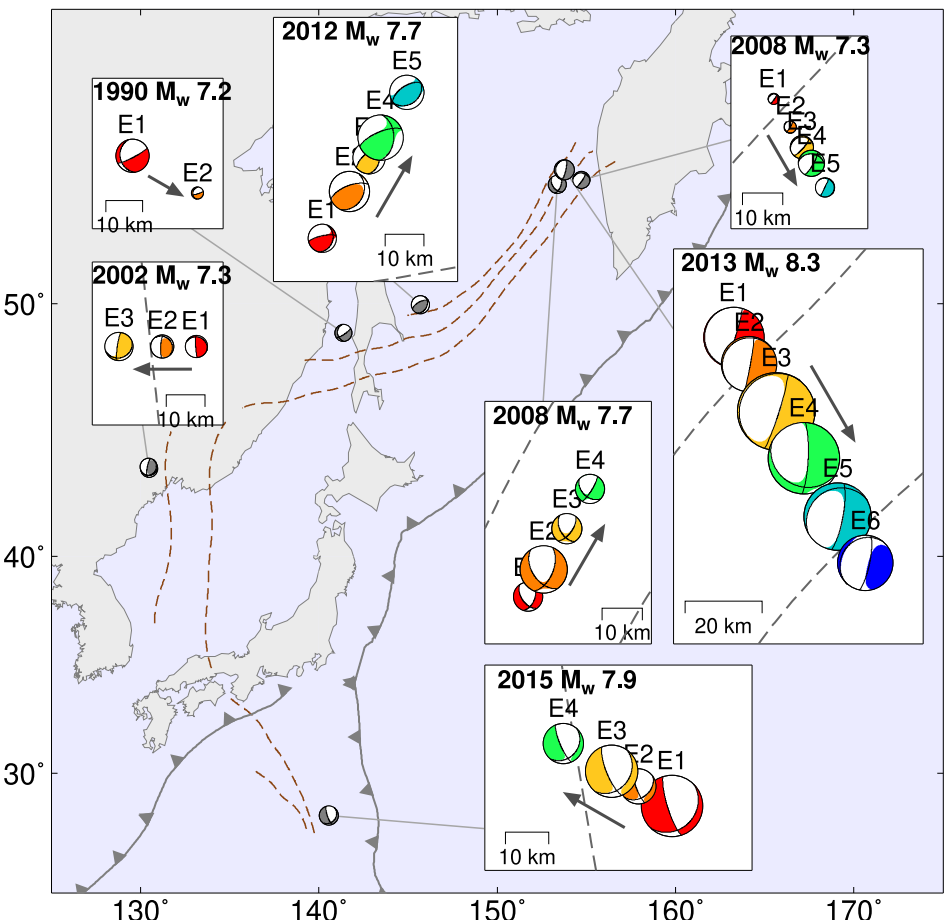


**Figure 2.** Subevent models of seven large deep earthquakes in the Kuril-Honshu-Bonin regions. Gray beachballs show the GCMT solutions for these events. Inset boxes show the subevent models for the corresponding earthquakes, where beachballs indicate the focal mechanisms and locations of subevents. The size of each subevent beachball is scaled proportionally to its seismic moment. Gray arrows indicate the inferred rupture directivity for each earthquake, pointing in the direction of rupture propagation. The color of each subevent beachball represents its timing in the rupture sequence (from early to late). Slab depth contours are from the Slab 2 model (Hayes et al., 2018).

et al., 2020; Tibi et al., 1999), and the results are generally consistent with a sub-horizontal rupture style (Figure S2 in Supporting Information S1). Additionally, we evaluate the influence of the vertical rupture extent, finding that it does not significantly affect our MOW analyses, which are discussed in more detail later. Robust estimates of the horizontal rupture length are critical for comparisons with the metastable olivine wedge geometry and assessing likely faulting mechanisms.

We find that 32 of the 40 target earthquakes require two or more subevents to explain their teleseismic body waves (Figures 2–5 and Figure S3 in Supporting Information S1). Subevent models suggest that the ruptures frequently penetrated through the interior of the slabs rather than being confined to the plate interface, such as for the 2013 Okhotsk  $M_w$  8.3 (Figure 2), the 1994  $M_w$  7.5 and 2018  $M_w$  8.2 Fiji deep earthquakes (Figure 3), and the 1994  $M_w$  8.2 Bolivia earthquake (Figure 5). The rupture lengths of these earthquakes vary from 10 to 70 km (Figures 2–5, Figure S3 in Supporting Information S1), and the associated rupture velocities range from 1 to 5 km/s (Figures S4 and S5 in Supporting Information S1). For example, the 1994 Fiji  $M_w$  7.5 earthquake ruptured approximately 30 km with a fast rupture speed of 4 km/s (Figure 3 and Figure S5 in Supporting Information S1), while the 1994 Bolivia  $M_w$  8.2 earthquake broke a fault area spanning approximately 20 km at a much slower rupture speed of 1 km/s (Figure 5). The seismic moment of the 1994 Bolivia earthquake was 10 times that of the 1994 Fiji earthquake. The larger moment for the Bolivia event, occurring over a smaller fault dimension, implies a stress drop about 30 times greater than that of the Fiji earthquake, suggesting different rupture dynamics of these events.

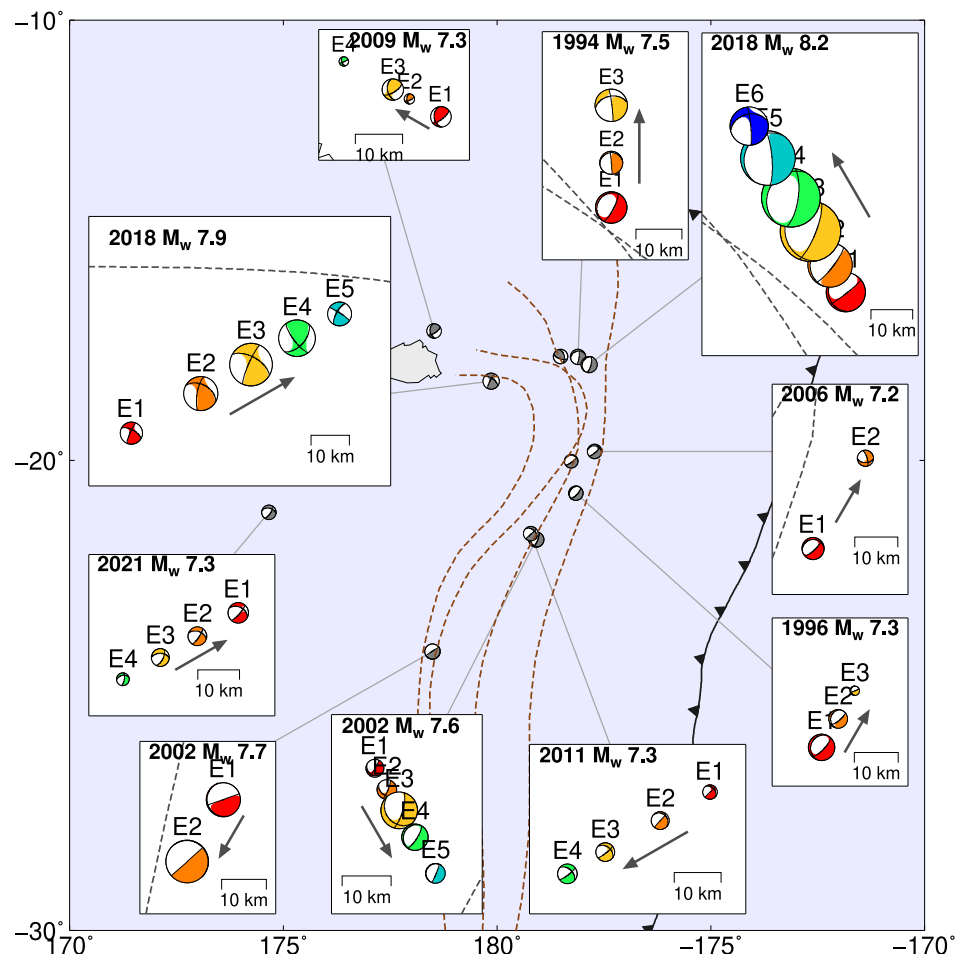


**Figure 3.** Subevent models of 11 large deep earthquakes in the Tonga subduction zone. Legends are similar to those in Figure 2, except that slab depth contours are from the RUM model (Gudmundsson & Sambridge, 1998).

We find that focal mechanisms of subevents can vary significantly for individual large deep earthquakes (Figures 2–5). For example, the subevents can rotate their strike angles by over 50° for the 1994  $M_w$  7.5, 2018  $M_w$  8.2 and 7.9 Fiji-Tonga, and 1996  $M_w$  7.7 Flores Sea deep earthquakes (Figures 3 and 4). These subevent focal mechanism changes suggest that the earthquakes likely involved multiple episodes of rupture occurring on different faults with distinct geometries. We measure this variation in focal mechanisms of subevents for the 32 earthquakes with two or more subevents using their maximum 3D rotation angles between every pair of subevents (Kagan, 1991). We find that the focal mechanism rotation angle tends to increase with earthquake magnitude (Figure S5 in Supporting Information S1), suggesting that deep earthquakes of larger magnitudes may have been governed by different processes at the initiation and arresting stages.

Our subevent models agree with source models obtained using other data sets and techniques. The total seismic moment and the combined focal mechanisms of these subevents agree with the models from the Global Centroid-Moment-Tensor (GCMT) catalog (Ekström et al., 2012) (Figure S4 in Supporting Information S1). The total source durations inferred from the subevents also align well with the source time functions from the SCARDEC data set (Vallée & Douet, 2016) (Figure S4 in Supporting Information S1). Their horizontal rupture lengths are in agreement with those in previous case studies (Figure S2 in Supporting Information S1). To further understand the uncertainties in our earthquake models, we apply bootstrap resampling to estimate standard errors in the rupture velocity and length. We find the 90% confidence limits in rupture lengths are mostly within 20 km (Figure S5 in Supporting Information S1).

We compare the horizontal rupture length of the 31 events with known slab geometries to the surrounding MOW widths. We resolve the MOW widths by conducting thermal simulations for subducting slabs where these deep

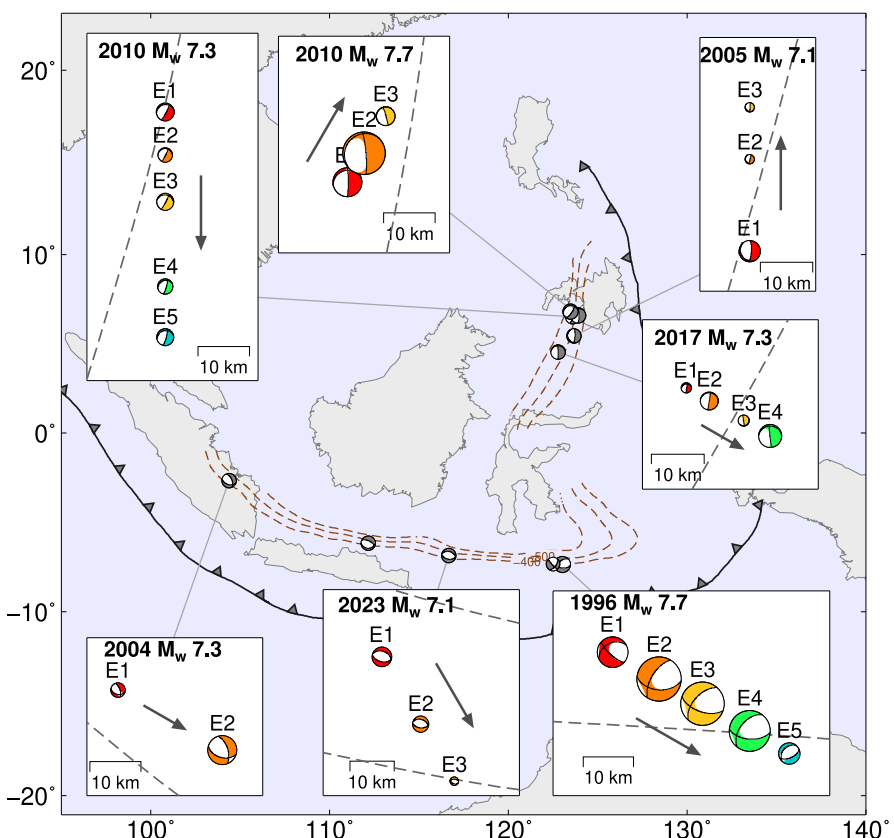


**Figure 4.** Subevent models of six large deep earthquakes in the Philippines and Sumatra subduction zones. Legends are similar to those in Figure 2.

earthquakes occurred, using a finite-element modeling method (Sime et al., 2024) and 2D cross section configurations specific for individual event (Figure S6 in Supporting Information S1). We take the 725°C isotherm as the blocking temperature to track the metastable olivine at these subducting slabs (Quinteros & Sobolev, 2012). This blocking temperature represents a warmer bound in previous estimations (Rubie & Ross II, 1994; Tetzlaff & Schmeling, 2000; Yoshioka et al., 2015), and decreasing this blocking temperature would yield thinner MOWs. Our simulations adopt realistic plate cooling model and other slab parameters, including geometries (Hayes et al., 2018), slab ages, mantle temperature adiabats, and convergence rate (Seton et al., 2012; Syracuse et al., 2010). The plate cooling model is used to account for the finite thickness of old oceanic lithosphere, and to incorporate mantle heat input for the lithosphere (Stein & Stein, 1992). We also consider scenarios using a half-space cooling model and a larger adiabatic temperature gradient to represent the cold and warm end members of slab thermal models, to assess the uncertainty range in evaluating MOW widths relative to deep earthquake rupture extents. Please see the Supporting Information S1 for more details (Brown & Shankland, 1981; Gudmundsson & Sambridge, 1998; Karato & Wu, 1993; Katsura et al., 2010; Leng & Mao, 2015; Stacey & Davis, 2008; Turcotte & Schubert, 2002; van Keken & Wilson, 2023a, 2023b; van Keken et al., 2008). Our simulations show that the MOW exists within cold subducting slabs and its thickness decreases with depth, consistent with previous studies (Kirby et al., 1996; Kawakatsu & Yoshioka, 2011; Marone & Liu, 1997; Shirey et al., 2021). At 550 km depth, we obtain a MOW thickness of 15, 16, 25, and 11 km for the Tonga, Kuril, Bonin, and Java-Banda Sea subduction slabs, respectively (Figures 6 and 7). Other warmer and younger subducting slabs, including the Honshu, Philippines, and South America slabs, have temperatures too high to permit coherent wedges of metastable olivine deeper than 500 km (Figure 6).

We find that 25 of the 31 earthquakes likely ruptured beyond the model-predicted MOW width (Figure 7), assuming the earthquakes initiated at the coldest core of the slab. Such a scenario was observed for the 2018 Fiji  $M_w$  8.2 earthquake, which nucleated near the slab core and ruptured out of the MOW (Fan et al., 2019; Jia, Shen, et al., 2020). If we assume that the earthquakes started at one MOW edge and ruptured toward the other end, 20

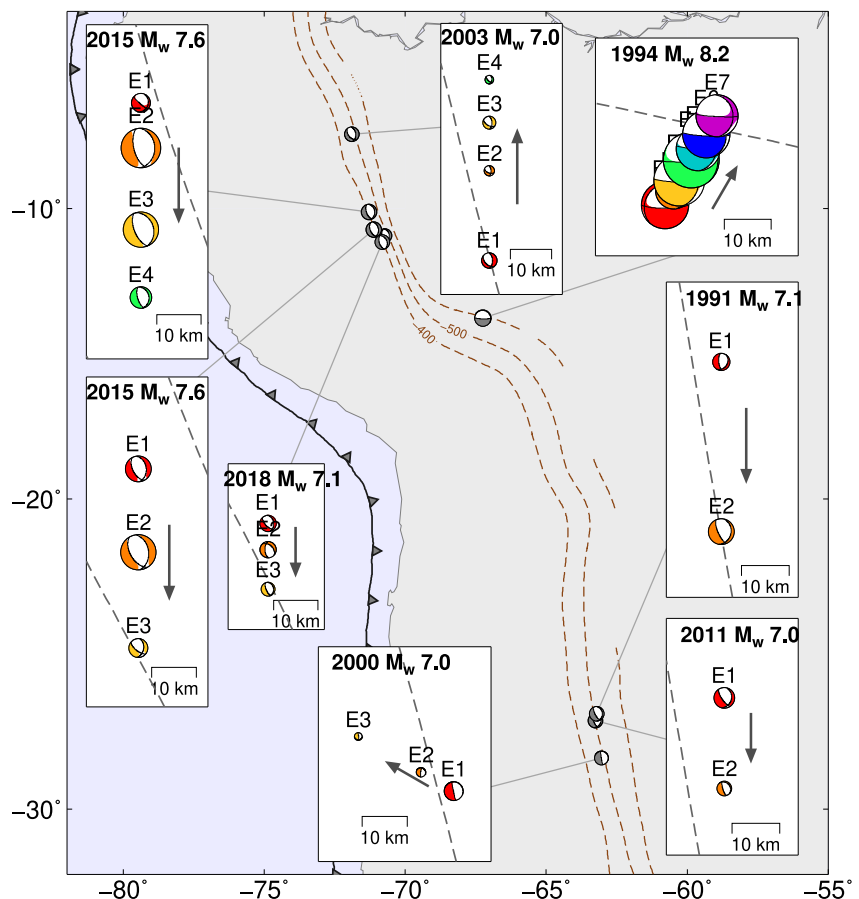


**Figure 5.** Subevent models of eight large deep earthquakes in the southern America subduction zone. Legends are similar to those in Figure 2.

earthquakes would have ruptured beyond the entire MOW width (Figure 7g). For example, the 2013 Okhotsk M<sub>w</sub> 8.3 earthquake ruptured approximately 65 km horizontally across the slab, four times greater than the predicted MOW thickness at a depth of 550 km. These events likely ruptured through the metastable olivine phase-transition boundary and extended into a thermal halo around the MOW, where ruptures appear to be able to propagate but earthquake nucleation may be prohibited (Figures 7d and 7e). In warm slabs deficient in MOWs, such as the South American slab, the slab temperature and composition are highly heterogeneous, possibly aided by an abrupt increase in the age of the subducted slab at depths of 300–500 km (Collier & Helffrich, 2001; Engebretson & Kirby, 1992; Kirby et al., 1995; Leite Neto et al., 2024, 2025). These heterogeneities may allow colder slab temperatures sporadically below these depths, leading to pockets of MOW where conditions are favorable. Earthquakes like the 1994 M<sub>w</sub> 8.2 Bolivia event may nucleate at such isolated MOW pockets (Brudzinski & Chen, 2005; Okal & Kirby, 1998; Tetzlaff & Schmeling, 2009; Vidale & Benz, 1992) and propagate into regions devoid of metastable olivine (Figure 7f). For such earthquakes, mechanisms other than transformational faulting, possibly shear melting, are likely driving their rupture propagation.

Both the earthquake rupture extent and the width of metastable olivine wedges (MOW) estimates can have uncertainties. We systematically evaluate these uncertainties and find that they do not substantially impact our main conclusion that ruptures of large deep earthquakes extend beyond the MOWs. First, potential up-dip or down-dip rupture of deep events might complicate comparisons of ruptures and MOWs. Previous studies indicate that large deep earthquake ruptures typically extend less than 20 km in depth (for example, Chen & Wen, 2015; Tibi et al., 2003). We incorporate this extent into our analysis, and find neither shallow nor downward ruptures significantly impact our observations of ruptures exceeding the MOWs (Figure S9 in Supporting Information S1). Second, the blocking temperature for olivine metastability remains controversial with estimates ranging from 660°C (Rubie & Ross II, 1994) to the 725°C (used in this study; Tetzlaff & Schmeling, 2000; Yoshioka

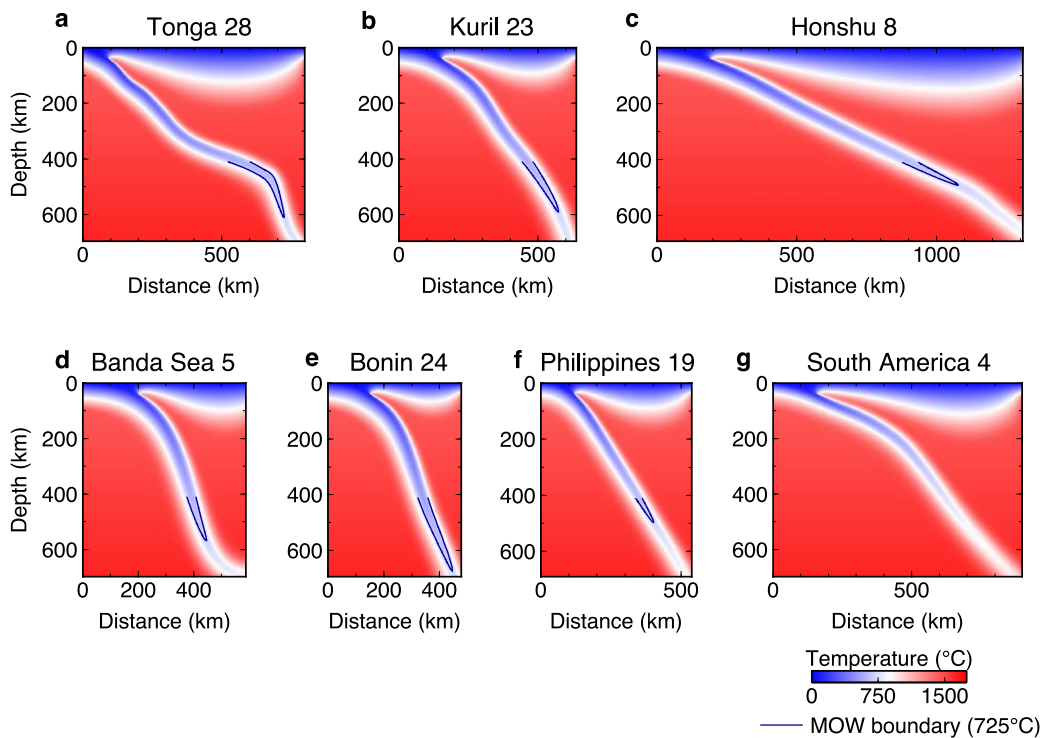


**Figure 6.** Thermal models of seven subduction slabs. These models have a mantle temperature of 1,450°C with an adiabatic gradient of 0.3°C/km. Numbers correspond to 2D transects in Figure S6 of Supporting Information S1. Blue lines indicate the inferred boundary for a 99% metastable olivine phase transformation, based on a blocking temperature of 725°C.

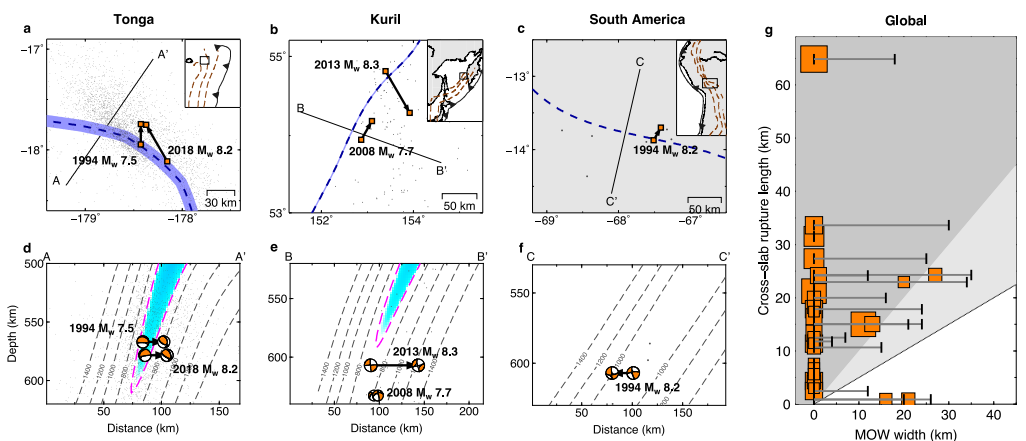


**Figure 7.** Examples of large deep earthquakes that rupture beyond the metastable olivine wedges. (a–c) Map views showing the rupture extents of large deep earthquakes (marked by orange squares for initiating and ending subevents) and the metastable olivine wedge (MOW) (blue belts) at 600 km depth in (a) Tonga, (b) Kuril, and (c) South America. Dashed blue lines represent the inferred coldest slab cores based on the RUM (for Tonga) and slab2 (for other slabs) contours at a depth of 600 km. Gray dots denote historical seismicity in these regions. (d–f) Cross-section views of the rupture extents (beachballs connected by arrows) and the MOW (blue colored area). Dashed gray lines represent isotherm contours from thermal simulations. (g) Large deep earthquake rupture extents and the metastable olivine wedge width. The cross-slab rupture dimension is determined by projecting the rupture length perpendicular to the local slab strike (Y-axis), and metastable olivine wedge widths (X-axis) are inferred from thermal models. Each earthquake is represented by an orange square with size proportional to the moment magnitude. The error bars indicate the MOW widths as derived from the cold and warm end-member slab models. The gray area highlights events with rupture extents that exceed the full width of the MOW. The light gray area indicates events that would have ruptured outside the MOWs if they nucleated at the MOW center.

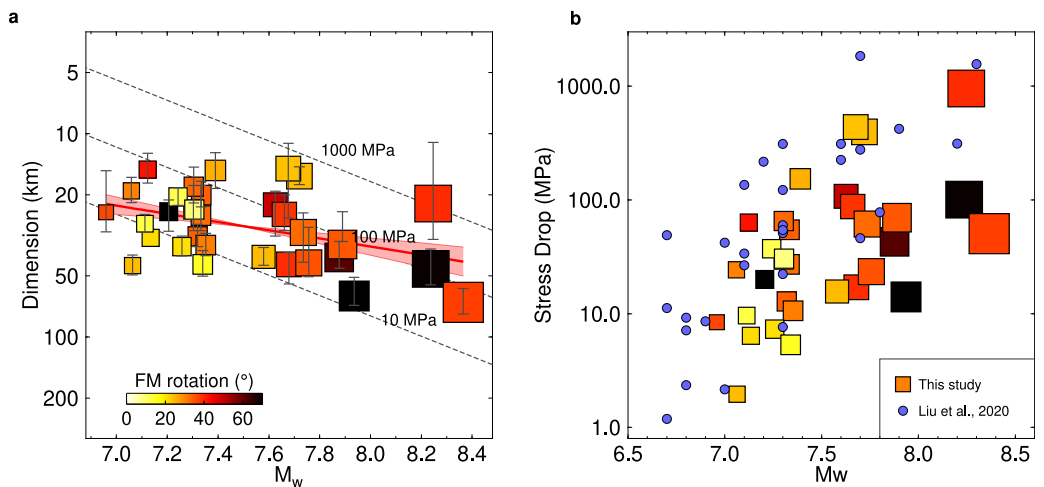


**Figure 8.** Increasing stress drop with magnitude for large deep earthquakes (squares), in which size is proportional to moment magnitude. (a) Relationship between rupture dimensions and moment magnitude ( $M_w$ ), shown as colored squares. Solid black lines on each square indicate the uncertainty of rupture dimensions (90% confidence interval) estimated with bootstrap resampling. Dashed lines represent predictions from self-similar circular rupture models. Orange line indicates a linear fit to the observed trend, with the surrounding colored area illustrating the standard deviation of the slope of this fit. The color intensity of each square reflects the 3D rotation angle of subevent focal mechanisms for each event. (b) Estimated stress drops of deep earthquakes as a function of their moment magnitude, based on a homogeneous circular rupture model. The observed trend aligns with measurements from Liu et al. Liu et al. (2020) (blue circles), showing a consistent pattern of increasing stress drop with magnitude across different analyses.

et al., 2015). Adopting a lower blocking temperature of  $660^{\circ}\text{C}$  leads to thinner MOWs (Figure S10 in Supporting Information S1), thereby increasing the observed discrepancies between rupture dimensions and MOWs. Finally, a  $\pm 20$  Ma variation in plate age does not significantly change the MOW widths (Figure S12 in Supporting Information S1). Using a half-space cooling model results in cooler temperatures and thicker MOWs than the plate cooling model used here, and applying an adiabatic gradient of  $0.5^{\circ}\text{C}/\text{km}$  yields warmer temperatures and thinner MOWs than the  $0.3^{\circ}\text{C}/\text{km}$  used in this study. Considering all these possible variations (Figure 7g), our simulations indicate that the MOWs under both warm and cold thermal scenarios are insufficient to accommodate the observed deep earthquake rupture extents.

### 3. Dual Mechanism Transition From Transformational Faulting to Thermal Runaway Enables Larger Final Magnitude of Deep Earthquakes

Our observations indicate that  $M > 7$  deep earthquakes are nucleated by the transformational faulting mechanism and transition to being governed by the thermal runaway process after their rupture propagates beyond the metastable olivine wedge. This transition process enables a larger final magnitude for these events. Deep earthquakes most likely nucleate by phase transitions of metastable olivine, as large deep earthquake sequences often show brittle-like characteristics by starting their ruptures with high rupture speed, high radiation efficiency, and moderate stress drop (Fan et al., 2019; Jia, Shen, et al., 2020; Meng et al., 2014; Ye et al., 2013; Zhan et al., 2014). Thermal runaway is unlikely to be a common initiating process for deep earthquakes because of a lack of a spontaneous mechanism for self-localization of shear thermal instability (Ogawa, 1987; Kelemen & Hirth, 2007). However, the thermal halo region is likely critically stressed as it is highly sensitive to external perturbations, where dynamic triggering of deep earthquakes occurs significantly more frequently than the MOW core (Luo & Wiens, 2020). Our results show that about half of the  $M > 7$  deep earthquakes occur in regions where slabs likely contain coherent MOW structures. We speculate that the rest of the events might initiate in isolated MOW pockets when no coherent MOW is present. However, once deep earthquakes rupture beyond the confining MOW (typically up to around 30 km thick) into regions exceeding blocking temperature for phase transition (around  $725^{\circ}\text{C}$ ), their rupture, if continued, can be sustained by weakening processes due to shear melting. Once the rupture crosses the MOW boundary, local stress heterogeneity may not align with the faults caused by phase transitions of metastable olivine. Consequently, rupture planes may deviate from their initial configurations, leading to larger variations in subevent focal mechanisms for earthquakes of greater magnitude (Figures 8 and 9).

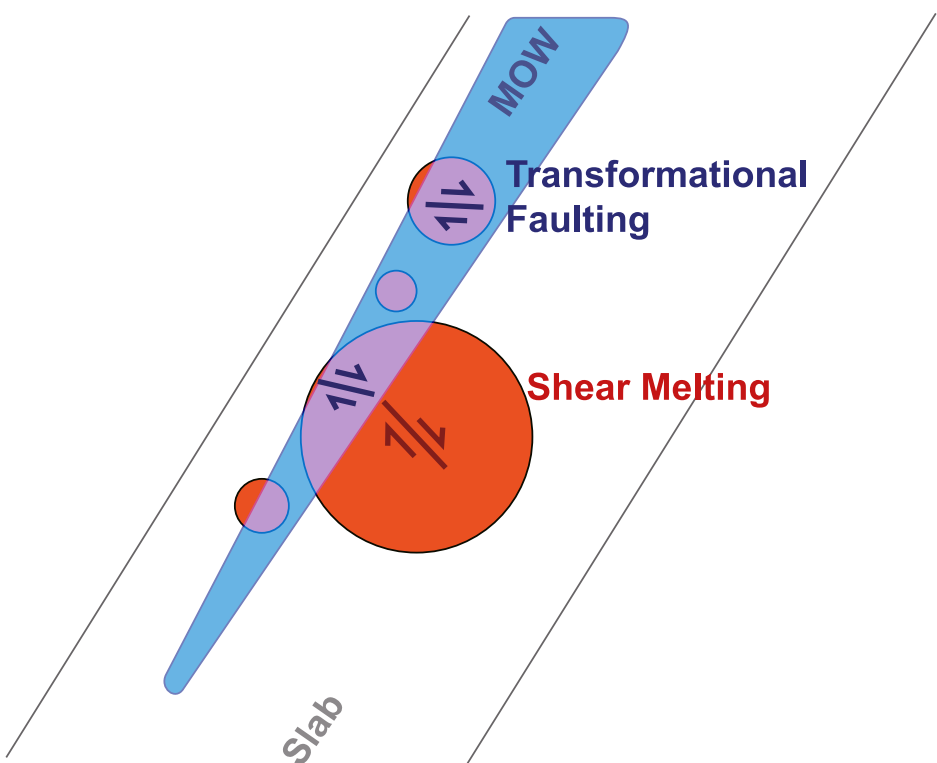


**Figure 9.** Schematic representation of rupture mechanisms of deep earthquakes with different magnitudes. Smaller events are likely confined within the MOW and dominated by the transformational-faulting mechanism. Their ruptures are characterized by lower stress drop and less geometric complexity. In contrast, larger earthquakes often rupture across the MOW boundary and transition to the shear thermal runaway mechanism with large slip and moment release outside the MOW. Consequently, they have characteristics of higher stress drop and greater geometric complexity.

Deep earthquakes caused by transformational faulting show moment release proportional to their size (Wang et al., 2017). This scaling relationship suggests that the transformational faulting process is comparable to brittle failure of shallow earthquakes (Cui et al., 2023; Li et al., 2018; Vallée, 2013). Consequently, deep earthquakes due to transformational faulting are likely to have little, if any, dependence of stress drop on moment. In contrast, the thermal runaway process can sustain earthquake rupture beyond the MOW boundary (thermal halo). However, the associated melting and large stress release could limit the rupture extent, and the moment release (earthquake slip) within the thermal halo is concentrated, disproportionate to its spatial length (Kanamori et al., 1998; Silver et al., 1995).

Our findings show that the total rupture lengths of 32 of the large deep earthquakes do not follow the moment-length scaling relationship typically observed in crustal earthquakes, suggesting their ruptures were not solely controlled by the transformational faulting mechanism (Figure 8). However, most of these earthquakes likely initiated in the cold slab cores, and this apparent paradox could be due to a dual control of both transformational faulting and thermal runaway mechanisms. The final earthquake magnitude hinges upon the transition of the mechanisms, and the transition is critical in releasing more moment and causing larger deep earthquakes ( $M > 7.5$ ). For smaller events (e.g.,  $M < 7.5$ ), their ruptures are confined within the associated MOWs and their stress drop is approximately 10 MPa (Figure 8). These stress drop estimates are comparable to those of crustal earthquakes (Houston & Williams, 1991; Shearer et al., 2022; Wiens et al., 1994). However, when earthquakes rupture beyond the MOW boundary and are sustained outside the MOW, they release most of their moment in the thermal halo, leading to larger magnitudes ( $M > 7.5$ ). Our models show that stress drops of  $M > 7.5$  deep earthquakes increase to 100 MPa on average, an order of magnitude greater than that of  $M < 7.5$  earthquakes (Figure 8). This difference between the smaller and larger events can also be seen in Figure S3 of Supporting Information S1; the average rupture length of the larger earthquakes is less than self-similar models' prediction based on the smaller earthquake rupture lengths, leading to bigger average stress drops for the larger earthquakes.

This stress drop–magnitude increase trend is robust to different assumptions for source scenarios (Figure S7 in Supporting Information S1). Specifically, we tested both circular and elliptical fault models (Kaneko & Shearer, 2015) with aspect ratios up to 2 and found that, although different rupture shapes can yield variations in the absolute stress drop estimates, up to three times higher than standard circular ones, the relative difference pattern remains the same, and the stress drop–magnitude relationship holds across all geometries. This stress drop pattern is also observed in global and Kuril deep earthquakes, whose stress drops estimates are independently obtained using different methods and data sets (Liu et al., 2020; Shi & Denolle, 2023; Turner et al., 2022). Additionally, we find that the horizontal rupture velocities of large, deep earthquakes are in the range of 20%–90% of the local shear wave velocity, different from the typical 50%–90% fraction of the shear wave velocity for shallow earthquakes (Figure S8 in Supporting Information S1). This difference is likely due to the partition of heat transfer and shear melting beyond the MOW boundary during the rupture processes of large deep earthquakes, where the rupture episodes due to thermal runaway might be slow, thereby reducing the average rupture velocity (Kanamori et al., 1998; Wiens, 2001; Tibi et al., 2003).

#### 4. Discussion and Conclusions

In addition to the transformational faulting and thermal runaway mechanisms, dehydration embrittlement has also been proposed to explain deep earthquakes (Meade & Jeanloz, 1991; Omori et al., 2004). However, this mechanism is challenged by the absence of an observable fluid release process (Green & Houston, 1995; Green et al., 2010). Petrological analysis of diamonds originating from the mantle transition zone finds inclusions of hydrous minerals, indicating the presence of water at these depths (Pearson et al., 2014; Shirey et al., 2021). However, water carried through the whole transition zone depths would be absorbed into the crystalline interfaces of the minerals, which do not migrate easily, causing the hydrous minerals to be stable for most slab conditions except regions with substantial slab folding and warming (Shirey et al., 2021). This stability of hydrous minerals renders dehydration embrittlement less plausible for causing deep earthquakes below 500 km (Green et al., 2010). In addition to metastable olivine, magnesite and enstatite may also transform into denser phases under the 500–700 km temperature and pressure conditions. These minerals, along with metastable olivine, might also be involved in transformational faulting (Hogrefe et al., 1994; Li et al., 2018). Among this suite of minerals, olivine is most abundant in the upper mantle, and laboratory experiments of olivine under realistic deep-earthquake conditions have successfully reproduced faulting, earthquake nucleation, the Gutenberg-Richter distribution, and predominantly deviatoric moment tensors (Schubnel et al., 2013; Wang et al., 2017). These findings support metastable olivine as the most likely mineral for the transformational faulting mechanism for deep earthquakes.

The Gutenberg-Richter b-value for global deep seismicity is approximately 1 (Zhan, 2017), similar to values observed for shallow earthquakes (El-Isa & Eaton, 2014; Frohlich & Davis, 1993). The b-value estimate predominantly reflects the characteristics of the abundant smaller earthquakes ( $M < 7$ ). If thermal runaway dominated these deep seismicity, a lower b-value ( $b < 1$ ) would be expected due to a lack of smaller events. Thus, the observed global average b-value around 1 (Zhan, 2017) implies that transformational faulting likely governs most small to intermediate-size deep earthquakes. This interpretation does not contradict the proposed dual-mechanism control of  $M > 7$  deep earthquakes, whose infrequent occurrence minimally impacts the global statistics. Additionally, reported regional contrasts in aftershock productivity and Gutenberg-Richter statistics between the cold Tonga and warm South America slabs (Wiens & Gilbert, 1996; Wiens, 2001; Zhan, 2017) further support the idea that the relative contributions of transformational faulting and shear thermal runaway vary with slab thermal structure. Collectively, our findings, along with the global statistics of deep seismicity, demonstrate that large and small deep earthquakes differ, with the larger events governed by the proposed dual mechanism transition.

Subduction dynamics at 500–700 km depth are reflected by the stress conditions within and around the subduction slabs (Alisic et al., 2010; Billen, 2008). Focal mechanisms are useful in inferring these stress conditions (Chang et al., 2019; Warren et al., 2015). However, the distribution of deep seismicity is associated with the extent of the MOW (Kirby et al., 1996). Despite occasional documented out-of-bound deep events (Kiser et al., 2021), the scarcity of seismic activity in the thermal halo outside of the MOW leaves the stress conditions at these parts of subduction slabs poorly understood. Our subevent models can provide a direct assessment of the moderate to small-scale stress environment in the thermal halos when deep earthquakes rupture beyond the MOWs. The focal mechanism rotations identified in our subevent models, spanning 10–70 km, agree in spatial pattern with the historical stress heterogeneities (Figure S11 in Supporting Information S1). This indicates that the focal mechanisms likely reflect the rupture's interaction with complex fault geometries (influenced by structural/

compositional boundaries, i.e. the MOW edge) and the heterogeneous stress environment with changes occurring over tens to hundreds of kilometers (Figure S11 in Supporting Information S1). These stress variations may arise from slab bending, structural heterogeneity, and adjacent mantle flow (Billen, 2020; Capitanio & Faccenda, 2012; Karato et al., 2001; Liu et al., 2021). Our observed stress rotations thus constrain the interplay between these thermo-mechanical boundary conditions and local stress fields, potentially aiding future numerical simulations for slab dynamics that account for more realistic stress environments and viscous resistance.

## Conflict of Interest

The authors declare no conflicts of interest relevant to this study.

## Data Availability Statement

All seismic data used in this study are publicly available from the IRIS-DMC. All subevent and thermal models are shown in the Supporting Information S1 and are publicly available at zenodo (Jia et al., 2025).

## Acknowledgments

The facilities of IRIS Data Services, and specifically the IRIS Data Management Center, were used for access to seismic waveforms recorded by global seismic networks II, IU, IC, G, GT, PS, the related metadata, and/or derived products used in this study. Our thermal model calculations were performed on the NSF ACCESS HPC clusters Stampede2 and Stampede3 at the Texas Advanced Computing Center (TACC) and Anvil at Purdue University. We thank Heidi Houston, Zhongwen Zhan, Lara Wagner, Alice Gabriel for helpful discussions. This work is supported by the United States Geological Survey Grant G22AP00011, and the Cecil and Ida Green Foundation. DM was supported by the National Science Foundation through Grant EAR-2121568 and OAC-2311208.

## References

- Alisic, L., Gurnis, M., Stadler, G., Burstedde, C., Wilcox, L. C., & Ghosh, O. (2010). Slab stress and strain rate as constraints on global mantle flow. *Geophysical Research Letters*, 37(22). <https://doi.org/10.1029/2010gl045312>
- Billen, M. I. (2008). Modeling the dynamics of subducting slabs. *Annual Review of Earth and Planetary Sciences*, 36(1), 325–356. <https://doi.org/10.1146/annurev.earth.36.031207.124129>
- Billen, M. I. (2020). Deep slab seismicity limited by rate of deformation in the transition zone. *Science Advances*, 6(22), eaaz7692. <https://doi.org/10.1126/sciadv.aaz7692>
- Brown, J. M., & Shankland, T. J. (1981). Thermodynamic parameters in the Earth as determined from seismic profiles. *Geophysical Journal International*, 66(3), 579–596. <https://doi.org/10.1111/j.1365-246X.1981.tb04891.x>
- Brudzinski, M. R., & Chen, W.-P. (2005). Earthquakes and strain in subhorizontal slabs. *Journal of Geophysical Research*, 110(B8). <https://doi.org/10.1029/2004jb003470>
- Burnley, P. C., Green, H. W., & Prior, D. J. (1991). Faulting associated with the olivine to spinel transformation in Mg<sub>2</sub>GeO<sub>4</sub> and its implications for deep-focus earthquakes. *Journal of Geophysical Research*, 96(B1), 425–443. <https://doi.org/10.1029/90jb01937>
- Capitanio, F. A., & Faccenda, M. (2012). Complex mantle flow around heterogeneous subducting oceanic plates. *Earth and Planetary Science Letters*, 353, 29–37. <https://doi.org/10.1016/j.epsl.2012.07.042>
- Chang, Y., Warren, L., Zhu, L., & Prieto, G. (2019). Earthquake focal mechanisms and stress field for the intermediate-depth Cauca cluster, Colombia. *Journal of Geophysical Research: Solid Earth*, 124(1), 822–836. <https://doi.org/10.1029/2018jb016804>
- Chen, Y., & Wen, L. (2015). Global large deep-focus earthquakes: Source process and cascading failure of shear instability as a unified physical mechanism. *Earth and Planetary Science Letters*, 423, 134–144. <https://doi.org/10.1016/j.epsl.2015.04.031>
- Collier, J., & Helffrich, G. (2001). The thermal influence of the subducting slab beneath South America from 410 and 660 km discontinuity observations. *Geophysical Journal International*, 147(2), 319–329. <https://doi.org/10.1046/j.1365-246x.2001.00532.x>
- Cui, X., Li, Z., & Hu, Y. (2023). Similar seismic moment release process for shallow and deep earthquakes. *Nature Geoscience*, 16(5), 1–7. <https://doi.org/10.1038/s41561-023-01176-5>
- Ekström, G., Nettles, M., & Dziewoński, A. (2012). The global CMT project 2004–2010: Centroid-moment tensors for 13,017 earthquakes. *Physics of the Earth and Planetary Interiors*, 200, 1–9.
- El-Isa, Z. H., & Eaton, D. W. (2014). Spatiotemporal variations in the b-value of earthquake magnitude–frequency distributions: Classification and causes. *Tectonophysics*, 615, 1–11. <https://doi.org/10.1016/j.tecto.2013.12.001>
- Engebretson, D., & Kirby, S. (1992). Deep Nazca slab seismicity: Why is it so anomalous. *Eos, Transactions American Geophysical Union*, 73(43), 379.
- Fan, W., Shearer, P. M., & Gerstoft, P. (2014). Kinematic earthquake rupture inversion in the frequency domain. *Geophysical Journal International*, 199(2), 1138–1160. <https://doi.org/10.1093/gji/egu319>
- Fan, W., Wei, S. S., Tian, D., McGuire, J. J., & Wiens, D. A. (2019). Complex and diverse rupture processes of the 2018 Mw 8.2 and Mw 7.9 Tonga–Fiji deep earthquakes. *Geophysical Research Letters*, 46(5), 2434–2448. <https://doi.org/10.1029/2018gl080997>
- Frohlich, C. (1989). The nature of deep-focus earthquakes. *Annual Review of Earth and Planetary Sciences*, 17(1), 227–254. <https://doi.org/10.1146/annurev.earth.17.1.227>
- Frohlich, C. (2006). *Deep earthquakes*. Cambridge University Press.
- Frohlich, C., & Davis, S. D. (1993). Teleseismic b values; or, much ado about 1.0. *Journal of Geophysical Research*, 98(B1), 631–644. <https://doi.org/10.1029/92jb01891>
- Goes, S., & Ritsema, J. (1995). A broadband P wave analysis of the large deep Fiji Island and Bolivia earthquakes of 1994. *Geophysical Research Letters*, 22(16), 2249–2252. <https://doi.org/10.1029/95gl02011>
- Green, H. W., & Burnley, P. (1989). A new self-organizing mechanism for deep-focus earthquakes. *Nature*, 341(6244), 733–737. <https://doi.org/10.1038/341733a0>
- Green, H. W., Chen, W.-P., & Brudzinski, M. R. (2010). Seismic evidence of negligible water carried below 400-km depth in subducting lithosphere. *Nature*, 467(7317), 828–831. <https://doi.org/10.1038/nature09401>
- Green, H. W., & Houston, H. (1995). The mechanics of deep earthquakes. *Annual Review of Earth and Planetary Sciences*, 23(1), 169–213. <https://doi.org/10.1146/annurev.ea.23.050195.001125>
- Gudmundsson, Ó., & Sambridge, M. (1998). A Regionalized Upper Mantle (RUM) seismic model. *Journal of Geophysical Research*, 103(B4), 7121–7136. <https://doi.org/10.1029/97jb02488>
- Gutenberg, B., & Richter, C. F. (1956). Earthquake magnitude, intensity, energy, and acceleration: (Second paper). *Bulletin of the Seismological Society of America*, 46(2), 105–145. <https://doi.org/10.1785/bssa0460020105>

- Hayes, G. P., Moore, G. L., Portner, D. E., Hearne, M., Flamme, H., Furtney, M., & Smoczyk, G. M. (2018). Slab2, a comprehensive subduction zone geometry model. *Science*, 362(6410), 58–61. <https://doi.org/10.1126/science.aat4723>
- Hogrefe, A., Rubie, D., Sharp, T., & Seifert, F. (1994). Metastability of enstatite in deep subducting lithosphere. *Nature*, 372(6504), 351–353. <https://doi.org/10.1038/372351a0>
- Houston, H., & Williams, Q. (1991). Fast rise times and the physical mechanism of deep earthquakes. *Nature*, 352(6335), 520–522. <https://doi.org/10.1038/352520a0>
- Isacks, B., & Molnar, P. (1971). Distribution of stresses in the descending lithosphere from a global survey of focal-mechanism solutions of mantle earthquakes. *Reviews of Geophysics*, 9(1), 103–174. <https://doi.org/10.1029/rg009i001p00103>
- Jia, Z., Fan, W., Mao, W., Shearer, P., & May, D. (2025). Subevent models and thermal simulation profiles for global M7+ deep earthquakes from 1990–2023 [Dataset]. <https://doi.org/10.5281/zenodo.15263621>
- Jia, Z., Shen, Z., Zhan, Z., Li, C., Peng, Z., & Gurnis, M. (2020). The 2018 Fiji Mw 8.2 and 7.9 deep earthquakes: One doublet in two slabs. *Earth and Planetary Science Letters*, 531(115), 997.
- Jia, Z., Wang, X., & Zhan, Z. (2020). Multifault models of the 2019 Ridgecrest sequence highlight complementary slip and fault junction instability. *Geophysical Research Letters*, 47(17), e2020GL089802. <https://doi.org/10.1029/2020gl089802>
- Jia, Z., Zhan, Z., & Kanamori, H. (2022). The 2021 South Sandwich Island Mw 8.2 earthquake: A slow event sandwiched between regular ruptures. *Geophysical Research Letters*, 49(3), e2021GL097104. <https://doi.org/10.1029/2021gl097104>
- Kagan, Y. (1991). 3-D rotation of double-couple earthquake sources. *Geophysical Journal International*, 106(3), 709–716. <https://doi.org/10.1111/j.1365-246x.1991.tb06343.x>
- Kanamori, H., Anderson, D. L., & Heaton, T. H. (1998). Frictional melting during the rupture of the 1994 Bolivian earthquake. *Science*, 279(5352), 839–842. <https://doi.org/10.1126/science.279.5352.839>
- Kaneko, Y., & Shearer, P. (2015). Variability of seismic source spectra, estimated stress drop, and radiated energy, derived from cohesive-zone models of symmetrical and asymmetrical circular and elliptical ruptures. *Journal of Geophysical Research: Solid Earth*, 120(2), 1053–1079. <https://doi.org/10.1002/2014jb011642>
- Karato, S., Riedel, M. R., & Yuen, D. A. (2001). Rheological structure and deformation of subducted slabs in the mantle transition zone: Implications for mantle circulation and deep earthquakes. *Physics of the Earth and Planetary Interiors*, 127(1–4), 83–108. [https://doi.org/10.1016/s0031-9201\(01\)00223-0](https://doi.org/10.1016/s0031-9201(01)00223-0)
- Karato, S. I., & Wu, P. (1993). Rheology of the upper mantle: A synthesis. *Science*, 260(5109), 771–778. <https://doi.org/10.1126/science.260.5109.771>
- Katsura, T., Yoneda, A., Yamazaki, D., Yoshino, T., & Ito, E. (2010). Adiabatic temperature profile in the mantle. *Physics of the Earth and Planetary Interiors*, 183(1), 212–218. <https://doi.org/10.1016/j.pepi.2010.07.001>
- Kawakatsu, H., & Yoshioka, S. (2011). Metastable olivine wedge and deep dry cold slab beneath Southwest Japan. *Earth and Planetary Science Letters*, 303(1–2), 1–10. <https://doi.org/10.1016/j.epsl.2011.01.008>
- Kelemen, P. B., & Hirth, G. (2007). A periodic shear-heating mechanism for intermediate-depth earthquakes in the mantle. *Nature*, 446(7137), 787–790. <https://doi.org/10.1038/nature05717>
- Kikuchi, M., & Kanamori, H. (1991). Inversion of complex body waves—III. *Bulletin of the Seismological Society of America*, 81(6), 2335–2350. <https://doi.org/10.1785/bssa0810062335>
- Kikuchi, M., & Kanamori, H. (1994). The mechanism of the deep Bolivia earthquake of June 9, 1994. *Geophysical Research Letters*, 21(22), 2341–2344. <https://doi.org/10.1029/94gl02483>
- Kirby, S. H. (1987). Localized polymorphic phase transformations in high-pressure faults and applications to the physical mechanism of deep earthquakes. *Journal of Geophysical Research*, 92(B13), 13789–13800. <https://doi.org/10.1029/jb092ib13p13789>
- Kirby, S. H., Okal, E. A., & Engdahl, E. R. (1995). The 9 June 94 Bolivian deep earthquake: An exceptional event in an extraordinary subduction zone. *Geophysical Research Letters*, 22(16), 2233–2236. <https://doi.org/10.1029/95gl01802>
- Kirby, S. H., Stein, S., Okal, E. A., & Rubie, D. C. (1996). Metastable mantle phase transformations and deep earthquakes in subducting oceanic lithosphere. *Reviews of Geophysics*, 34(2), 261–306. <https://doi.org/10.1029/96rg01050>
- Kiser, E., Kehoe, H., Chen, M., & Hughes, A. (2021). Lower mantle seismicity following the 2015 Mw 7.9 Bonin Islands deep-focus earthquake. *Geophysical Research Letters*, 48(13), e2021GL093111. <https://doi.org/10.1029/2021gl093111>
- Lay, T., Kanamori, H., Ammon, C. J., Koper, K. D., Hutko, A. R., Ye, L., et al. (2012). Depth-varying rupture properties of subduction zone megathrust faults. *Journal of Geophysical Research*, 117(B4). <https://doi.org/10.1029/2011jb009133>
- Leite Neto, G., Julià, J., & Prieto, G. (2024). Deep-focus earthquake mechanisms at the subducting Nazca plate (Peru-Brazil border): Cold slab behavior in a warm plate. *Earth and Space Science*, 11(10), e2024EA003617. <https://doi.org/10.1029/2024ea003617>
- Leite Neto, G., Prieto, G., & Julià, J. (2025). Deep-Focus earthquakes in warm slabs: Seismic source parameters in the Peru-Brazil region. *Journal of Geophysical Research: Solid Earth*, 130(2), e2024JB029900. <https://doi.org/10.1029/2024jb029900>
- Leng, W., & Mao, W. (2015). Geodynamic modeling of thermal structure of subduction zones. *Science China Earth Sciences*, 58(7), 1070–1083. <https://doi.org/10.1007/s11430-015-5107-5>
- Li, J., Zheng, Y., Thomsen, L., Lapen, T. J., & Fang, X. (2018). Deep earthquakes in subducting slabs hosted in highly anisotropic rock fabric. *Nature Geoscience*, 11(9), 696–700. <https://doi.org/10.1038/s41561-018-0188-3>
- Liu, H., Gurnis, M., Leng, W., Jia, Z., & Zhan, Z. (2021). Tonga slab morphology and stress variations controlled by a relic slab: Implications for deep earthquakes in the Tonga-Fiji Region. *Geophysical Research Letters*, 48(7), e2020GL091331. <https://doi.org/10.1029/2020gl091331>
- Liu, M., Huang, Y., & Ritsema, J. (2020). Stress drop variation of deep-focus earthquakes based on empirical Green's functions. *Geophysical Research Letters*, 47(9), e2019GL086055. <https://doi.org/10.1029/2019gl086055>
- Luo, Y., & Wiens, D. A. (2020). High rates of deep earthquake dynamic triggering in the thermal halos of subducting slabs. *Geophysical Research Letters*, 47(8), e2019GL086125. <https://doi.org/10.1029/2019gl086125>
- Marone, C., & Liu, M. (1997). Transformation shear instability and the seismogenic zone for deep earthquakes. *Geophysical Research Letters*, 24(15), 1887–1890. <https://doi.org/10.1029/97gl01851>
- McGuire, J. J., Wiens, D. A., Shore, P. J., & Bevis, M. G. (1997). The March 9, 1994 (Mw 7.6), deep Tonga earthquake: Rupture outside the seismically active slab. *Journal of Geophysical Research*, 102(B7), 15163–15182. <https://doi.org/10.1029/96jb03185>
- Meade, C., & Jeanloz, R. (1991). Deep-focus earthquakes and recycling of water into the Earth's mantle. *Science*, 252(5002), 68–72. <https://doi.org/10.1126/science.252.5002.68>
- Meng, L., Ampuero, J.-P., & Bürgmann, R. (2014). The 2013 Okhotsk deep-focus earthquake: Rupture beyond the metastable olivine wedge and thermally controlled rise time near the edge of a slab. *Geophysical Research Letters*, 41(11), 3779–3785. <https://doi.org/10.1002/2014gl059968>

- Mosenfelder, J. L., Marton, F. C., Ross, C. R., II, Kerschhofer, L., & Rubie, D. C. (2001). Experimental constraints on the depth of olivine metastability in subducting lithosphere. *Physics of the Earth and Planetary Interiors*, 127(1–4), 165–180. [https://doi.org/10.1016/s0031-9201\(01\)00226-6](https://doi.org/10.1016/s0031-9201(01)00226-6)
- Myhill, R. (2013). Slab buckling and its effect on the distributions and focal mechanisms of deep-focus earthquakes. *Geophysical Journal International*, 192(2), 837–853. <https://doi.org/10.1093/gji/ggs054>
- Nissen-Meyer, T., Van Driel, M., Stähler, S. C., Hosseini, K., Hempel, S., Auer, L., et al. (2014). AxiSEM: Broadband 3-D seismic wavefields in axisymmetric media. *Solid Earth*, 5(1), 425–445. <https://doi.org/10.5194/se-5-425-2014>
- Ogawa, M. (1987). Shear instability in a viscoelastic material as the cause of deep focus earthquakes. *Journal of Geophysical Research*, 92(B13), 13801–13810. <https://doi.org/10.1029/jb092ib13p13801>
- Okal, E. A., & Kirby, S. H. (1998). Deep earthquakes beneath the Fiji Basin, SW Pacific: Earth's most intense deep seismicity in stagnant slabs. *Physics of the Earth and Planetary Interiors*, 109(1–2), 25–63. [https://doi.org/10.1016/s0031-9201\(98\)00116-2](https://doi.org/10.1016/s0031-9201(98)00116-2)
- Omori, S., Komabayashi, T., & Maruyama, S. (2004). Dehydration and earthquakes in the subducting slab: Empirical link in intermediate and deep seismic zones. *Physics of the Earth and Planetary Interiors*, 146(1–2), 297–311. <https://doi.org/10.1016/j.pepi.2003.08.014>
- Pearson, D., Brenker, F., Nestola, F., McNeill, J., Nasdala, L., Hutchison, M., et al. (2014). Hydrous mantle transition zone indicated by ring-woodite included within diamond. *Nature*, 507(7491), 221–224. <https://doi.org/10.1038/nature13080>
- Quinteros, J., & Sobolev, S. V. (2012). Constraining kinetics of metastable olivine in the Marianas slab from seismic observations and dynamic models. *Tectonophysics*, 526, 48–55. <https://doi.org/10.1016/j.tecto.2011.11.005>
- Rubie, D. C., & Ross, C. R., II. (1994). Kinetics of the olivine-spinel transformation in subducting lithosphere: Experimental constraints and implications for deep slab processes. *Physics of the Earth and Planetary Interiors*, 86(1–3), 223–243. [https://doi.org/10.1016/0031-9201\(94\)05070-8](https://doi.org/10.1016/0031-9201(94)05070-8)
- Schmeling, H., Monz, R., & Rubie, D. C. (1999). The influence of olivine metastability on the dynamics of subduction. *Earth and Planetary Science Letters*, 165(1), 55–66. [https://doi.org/10.1016/s0012-821x\(98\)00249-0](https://doi.org/10.1016/s0012-821x(98)00249-0)
- Schubnel, A., Brunet, F., Hilairet, N., Gasc, J., Wang, Y., & Green, H. W. (2013). Deep-focus earthquake analogs recorded at high pressure and temperature in the laboratory. *Science*, 341(6152), 1377–1380. <https://doi.org/10.1126/science.1240206>
- Seton, M., Müller, R. D., Zahirovic, S., Gaina, C., Torsvik, T., Shephard, G., et al. (2012). Global continental and ocean basin reconstructions since 200 Ma. *Earth-Science Reviews*, 113(3–4), 212–270. <https://doi.org/10.1016/j.earscirev.2012.03.002>
- Shearer, P. M., Abercrombie, R. E., & Trugman, D. T. (2022). Improved stress drop estimates for M 1.5 to 4 earthquakes in southern California from 1996 to 2019. *Journal of Geophysical Research: Solid Earth*, 127(7), e2022JB024243. <https://doi.org/10.1029/2022jb024243>
- Shen, Z., & Zhan, Z. (2020). Metastable olivine wedge beneath the Japan Sea imaged by seismic interferometry. *Geophysical Research Letters*, 47(6), e2019GL085665. <https://doi.org/10.1029/2019gl085665>
- Shi, Q., & Denolle, M. A. (2023). Improved observations of deep earthquake ruptures using machine learning. *Journal of Geophysical Research: Solid Earth*, 128(12), e2023JB027334. <https://doi.org/10.1029/2023jb027334>
- Shi, Q., Wei, S., & Chen, M. (2018). An MCMC multiple point sources inversion scheme and its application to the 2016 Kumamoto Mw 6.2 earthquake. *Geophysical Journal International*, 215(2), 737–752. <https://doi.org/10.1093/gji/ggy302>
- Shirey, S. B., Wagner, L. S., Walter, M. J., Pearson, D. G., & van Keeken, P. E. (2021). Slab transport of fluids to deep focus earthquake depths—thermal modeling constraints and evidence from diamonds. *AGU Advances*, 2(2), e2020AV000304. <https://doi.org/10.1029/2020av000304>
- Silver, P. G., Beck, S. L., Wallace, T. C., Meade, C., Myers, S. C., James, D. E., & Kuehnel, R. (1995). Rupture characteristics of the deep Bolivian earthquake of 9 June 1994 and the mechanism of deep-focus earthquakes. *Science*, 268(5207), 69–73. <https://doi.org/10.1126/science.268.5207.69>
- Sime, N., Wilson, C. R., & van Keeken, P. E. (2024). Thermal modeling of subduction zones with prescribed and evolving 2D and 3D slab geometries. *Progress in Earth and Planetary Science*, 11(1), 14. <https://doi.org/10.1186/s40645-024-00611-4>
- Stacey, F. D., & Davis, P. M. (2008). *Physics of the Earth*. Cambridge University Press.
- Stein, C. A., & Stein, S. (1992). A model for the global variation in oceanic depth and heat flow with lithospheric age. *Nature*, 359(6391), 123–129. <https://doi.org/10.1038/359123a0>
- Syracuse, E. M., van Keeken, P. E., & Abers, G. A. (2010). The global range of subduction zone thermal models. *Physics of the Earth and Planetary Interiors*, 183(1–2), 73–90. <https://doi.org/10.1016/j.pepi.2010.02.004>
- Tetzlaff, M., & Schmeling, H. (2000). The influence of olivine metastability on deep subduction of oceanic lithosphere. *Physics of the Earth and Planetary Interiors*, 120(1–2), 29–38. [https://doi.org/10.1016/s0031-9201\(00\)00139-4](https://doi.org/10.1016/s0031-9201(00)00139-4)
- Tetzlaff, M., & Schmeling, H. (2009). Time-dependent interaction between subduction dynamics and phase transition kinetics. *Geophysical Journal International*, 178(2), 826–844. <https://doi.org/10.1111/j.1365-246x.2009.04182.x>
- Tibi, R., Bock, G., & Wiens, D. A. (2003). Source characteristics of large deep earthquakes: Constraint on the faulting mechanism at great depths. *Journal of Geophysical Research*, 108(B2). <https://doi.org/10.1029/2002jb001948>
- Tibi, R., Estabrook, C., & Bock, G. (1999). The 1996 June 17 Flores Sea and 1994 March 9 Fiji-Tonga earthquakes: Source processes and deep earthquake mechanisms. *Geophysical Journal International*, 138(3), 625–642. <https://doi.org/10.1046/j.1365-246x.1999.00879.x>
- Turcotte, D. L., & Schubert, G. (2002). *Geodynamics* (2 ed.). Cambridge University Press. <https://doi.org/10.1017/CBO9780511807442>
- Turner, A. R., Ferreira, A. M., Berbellini, A., Brantut, N., Facenna, M., & Kendall, E. (2022). Across-slab propagation and low stress drops of deep earthquakes in the Kuril subduction zone. *Geophysical Research Letters*, 49(16), e2022GL098402. <https://doi.org/10.1029/2022gl098402>
- Vallée, M. (2013). Source time function properties indicate a strain drop independent of earthquake depth and magnitude. *Nature Communications*, 4(1), 2606. <https://doi.org/10.1038/ncomms3606>
- Vallée, M., & Douet, V. (2016). A new database of Source Time Functions (STFs) extracted from the SCARDEC method. *Physics of the Earth and Planetary Interiors*, 257, 149–157. <https://doi.org/10.1016/j.pepi.2016.05.012>
- Van Driel, M., Krischer, L., Stähler, S. C., Hosseini, K., & Nissen-Meyer, T. (2015). Instaseis: Instant global seismograms based on a broadband waveform database. *Solid Earth*, 6(2), 701–717. <https://doi.org/10.5194/se-6-701-2015>
- van Keeken, P. E., Currie, C., King, S. D., Behn, M. D., Cagnioncle, A., He, J., et al. (2008). A community benchmark for subduction zone modeling. *Physics of the Earth and Planetary Interiors*, 171(1), 187–197. <https://doi.org/10.1016/j.pepi.2008.04.015>
- van Keeken, P. E., & Wilson, C. R. (2023a). An introductory review of the thermal structure of subduction zones: I—motivation and selected examples. *Progress in Earth and Planetary Science*, 10(1), 42. <https://doi.org/10.1186/s40645-023-00573-z>
- van Keeken, P. E., & Wilson, C. R. (2023b). An introductory review of the thermal structure of subduction zones: III—Comparison between models and observations. *Progress in Earth and Planetary Science*, 10(1), 57. <https://doi.org/10.1186/s40645-023-00589-5>
- Vidale, J. E., & Benz, H. M. (1992). Upper-mantle seismic discontinuities and the thermal structure of subduction zones. *Nature*, 356(6371), 678–683. <https://doi.org/10.1038/356678a0>

- Wang, Y., Zhu, L., Shi, F., Schubnel, A., Hilairet, N., Yu, T., et al. (2017). A laboratory nanoseismological study on deep-focus earthquake micromechanics. *Science Advances*, 3(7), e1601896. <https://doi.org/10.1126/sciadv.1601896>
- Warren, L. M., Baluyut, E. C., Osburg, T., Lisac, K., & Kokkinen, S. (2015). Fault plane orientations of intermediate-depth and deep-focus earthquakes in the Japan-Kuril-Kamchatka subduction zone. *Journal of Geophysical Research: Solid Earth*, 120(12), 8366–8382. <https://doi.org/10.1002/2015jb012463>
- Wei, S., Helmberger, D., Zhan, Z., & Graves, R. (2013). Rupture complexity of the Mw 8.3 Sea of Okhotsk earthquake: Rapid triggering of complementary earthquakes? *Geophysical Research Letters*, 40(19), 5034–5039. <https://doi.org/10.1002/grl.50977>
- Wiens, D. A. (2001). Seismological constraints on the mechanism of deep earthquakes: Temperature dependence of deep earthquake source properties. *Physics of the Earth and Planetary Interiors*, 127(1–4), 145–163. [https://doi.org/10.1016/s0031-9201\(01\)00225-4](https://doi.org/10.1016/s0031-9201(01)00225-4)
- Wiens, D. A., & Gilbert, H. J. (1996). Effect of slab temperature on deep-earthquake aftershock productivity and magnitude–frequency relations. *Nature*, 384(6605), 153–156. <https://doi.org/10.1038/384153a0>
- Wiens, D. A., McGuire, J. J., Shore, P. J., Bevis, M. G., Draudinalo, K., Prasad, G., & Helu, S. P. (1994). A deep earthquake aftershock sequence and implications for the rupture mechanism of deep earthquakes. *Nature*, 372(6506), 540–543. <https://doi.org/10.1038/372540a0>
- Yao, H., Gerstoft, P., Shearer, P. M., & Mecklenbräuker, C. (2011). Compressive sensing of the Tohoku-Oki Mw 9.0 earthquake: Frequency-dependent rupture modes. *Geophysical Research Letters*, 38(20). <https://doi.org/10.1029/2011GL049223>
- Ye, L., Lay, T., Kanamori, H., & Koper, K. D. (2013). Energy release of the 2013 Mw 8.3 Sea of Okhotsk earthquake and deep slab stress heterogeneity. *Science*, 341(6152), 1380–1384. <https://doi.org/10.1126/science.1242032>
- Ye, L., Lay, T., Zhan, Z., Kanamori, H., & Hao, J.-L. (2016). The isolated 680 km deep 30 may 2015 Mw 7.9 Ogasawara (bonin) islands earthquake. *Earth and Planetary Science Letters*, 433, 169–179. <https://doi.org/10.1016/j.epsl.2015.10.049>
- Yoshioka, S., Torii, Y., & Riedel, M. R. (2015). Impact of phase change kinetics on the Mariana slab within the framework of 2-D mantle convection. *Physics of the Earth and Planetary Interiors*, 240, 70–81. <https://doi.org/10.1016/j.pepi.2014.12.001>
- Yue, H., & Lay, T. (2020). Resolving complicated faulting process using multi-point-source representation: Iterative inversion algorithm improvement and application to recent complex earthquakes. *Journal of Geophysical Research: Solid Earth*, 125(2), e2019JB018601. <https://doi.org/10.1029/2019jb018601>
- Zhan, Z. (2017). Gutenberg–Richter law for deep earthquakes revisited: A dual-mechanism hypothesis. *Earth and Planetary Science Letters*, 461, 1–7. <https://doi.org/10.1016/j.epsl.2016.12.030>
- Zhan, Z. (2020). Mechanisms and implications of deep earthquakes. *Annual Review of Earth and Planetary Sciences*, 48(1), 147–174. <https://doi.org/10.1146/annurev-earth-053018-060314>
- Zhan, Z., Kanamori, H., Tsai, V. C., Helmberger, D. V., & Wei, S. (2014). Rupture complexity of the 1994 Bolivia and 2013 Sea of Okhotsk deep earthquakes. *Earth and Planetary Science Letters*, 385, 89–96. <https://doi.org/10.1016/j.epsl.2013.10.028>

## References From the Supporting Information

- Ye, L., Lay, T., Kanamori, H., Zhan, Z., & Duputel, Z. (2016b). Diverse rupture processes in the 2015 Peru deep earthquake doublet. *Science Advances*, 2(6), e1600581. <https://doi.org/10.1126/sciadv.1600581>